Effects of Grain Slots on Flow in a Solid Rocket Motor

R. H. W. Waesche*
Atlantic Research Corporation, Gainesville, Virginia 22065
and
J. F. Marchman† and S. Kuppa‡
Virginia Polytechnic Institute and State University, Blacksburg, Virginia 24061

A series of cold-gas tests was conducted in ⅛-scale (18-in.-diam) models of the forward segment of candidate grain designs for the Advanced Solid Rocket Motor. Models were fabricated which represented the grain surface, including mass injection, at two different burning times. The effects of grain geometry on the flow entering the forward center segment were evaluated; pressure, velocity, and turbulence profiles were determined at different axial stations. It was found that the effects of grain slots on the downstream flow dissipate quickly; there is rapid mixing with the core flow. More significantly, no significant localized flow impingement was observed on the face of the downstream grain segment. These findings imply that the effects of forward slots on downstream flow are minimal.

Introduction

FOR most solid rocket motor (SRM) grain designs, the burning surface must be tailored to achieve a specified thrust-time history. In many current designs, the forward section of the grain employs a noncylindrical geometry, usually for ease in insulation design or for maintenance of a specified center of mass. Examples of such designs are finocyls (fins incorporated in the forward end) or conocyls (conical sections of propellant removed in the forward end). For instance, the Titan III 120-in. SRM employs a forward-segment, slotted-grain concept.

The grain design employed in the current Space Shuttle booster (SRB) contains slots in the forward end of the grain to achieve a desired thrust-time behavior. Adding further complexity to the SRB flowfield are joints separating the four grain segments of the SRB. Design of the insulation at the forward end of the second segment is made more complex by the flow from the upstream slots. There is concern that the local burning rate of the solid propellant in this region of the SRB is affected by local variations in the flow over the burning grain, even though mean velocities are low. This concern is lessened by the history of the Titan III, which has indicated that such local variations were not sufficient to affect motor performance significantly.

The most detailed descriptions of solid-rocket internal flow fields have been obtained by Dunlap et al.[1] and Brown et al.[2] In their studies, nitrogen flowing through porous chamber walls was employed to simulate the flowfield in several chamber geometries. Mean and fluctuating components of the velocity were measured with three-element hot-wire anemometers. They found that mean velocity profiles before transition showed fair agreement with those derived for a rotational inviscid flow injected normal to the surface. Downstream of transition, velocity profiles became flatter in the core flow region. Other cold-flow tests were conducted in water by Waesche et al.,[3] who found circumferential flows existed in the aft dome and in the region between segments when any asymmetry existed in the motor geometry; these tests were qualitative in nature. Majumdor and Whitesides[4] made measurements of pressure distributions in these regions and used oil-film techniques to characterize local flow conditions. It was found that circumferential pressure drop with slotted inhi-

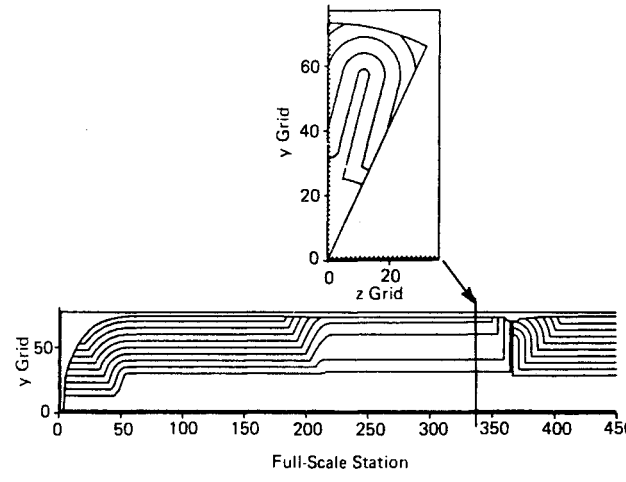

Fig. 1 Grain burnback patterns.

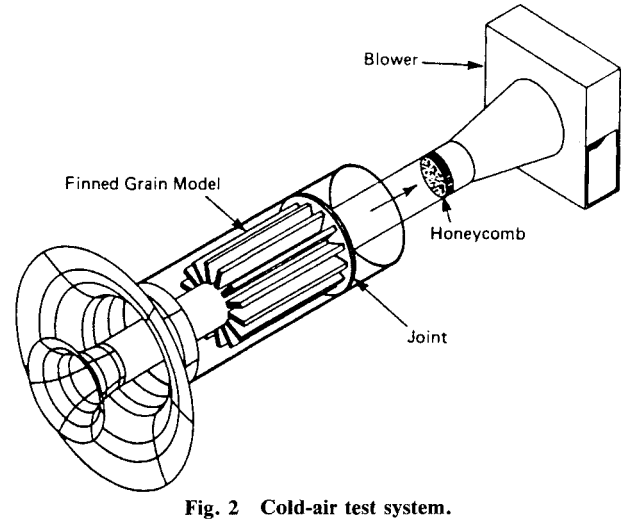

Fig. 2 Cold-air test system.

Received May 8, 1989; presented as Paper 89-2970 at the AIAA 25th Joint Propulsion Conference, Monterey, CA, July 10-13, 1989; revision received and accepted for publication May 22, 1990.

*Principal Scientist, Virginia Propulsion Division, 5945 Wellington Rd. Fellow AIAA.

†Associate Dean for Academic Affairs, School of Engineering. Associate Fellow AIAA.

‡Research Assistant; currently with Analytical Services and Materials, Inc., 107 Research Dr., Hampton, VA 23666.

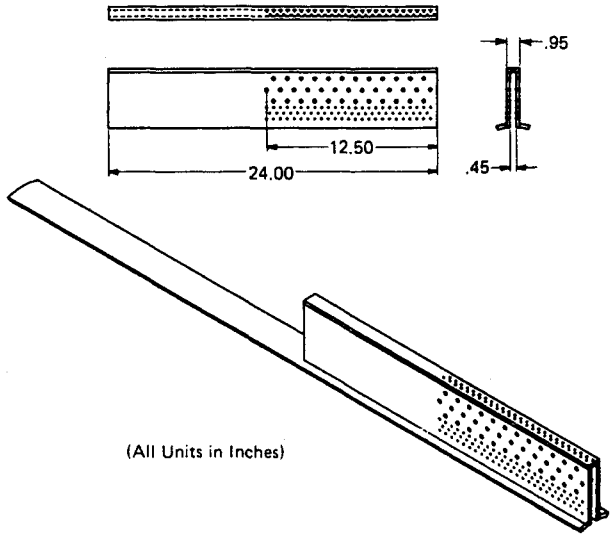

Fig. 3 Detail of model fin design and hole pattern.

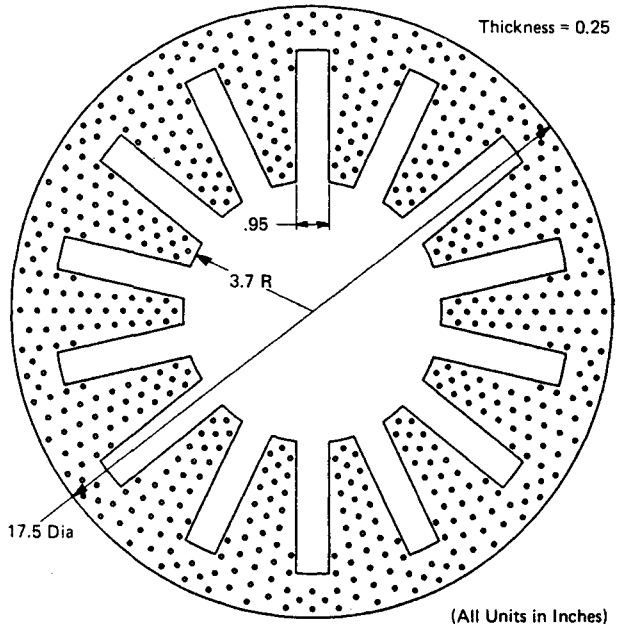

Fig. 4 Detail of end of first-segment grain model.

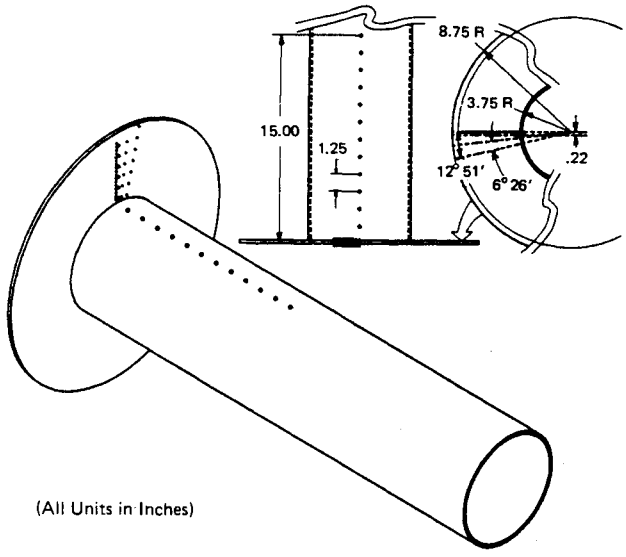

Fig. 5 Pressure tap placement in second-segment grain surface model.

bitors was a strong function of slot depth; the height of the inhibitor was also important. The FLUENT code was able to predict trends.

To aid in the design of potential candidate Advanced Solid Rocket Motor (ASRM) forward-slot grain designs, a cold-flow program was conducted to characterize the local flowfield in the region between the first and second segments of one such potential design at two different times in a firing. This paper discusses quantitative measurements of the local flowfield made in air. These tests were aimed at characterization of the flow impacting the face of the second-segment inhibitor, the pressure and velocity fields in the joint between the two segments, and the shape of the boundary layers at the aft end of the first segment and the forward end of the second segment.

A description of the experimental apparatus and of the tests conducted is presented, together with the test results and their implication for the motor designer.

Experimental Apparatus

These tests were conducted using cold-air flow through a model of the joint between the two forward segments of a candidate design for the Space Shuttle ASRM. The forward segment of the candidate design contains a finned or slotted (depending on one's perspective) grain that is followed by a simple cylindrical grain in the following segment of the SRM. Note that the upstream face of the downstream grain is inhibited against burning. Figure 1 shows the grain configurations on both sides of the joint with burnback lines indicated on the section and axial views. Also shown in Fig. 1 are the full-scale dimensions of the SRM grain. The station numbers in Fig. 1 represent the distance from the head end of the SRM; these station numbers will be employed in this paper to identify the axial location being studied.

Tests were run using models to simulate the grain surface at ignition and at 35 s into the SRM burning time. The primary objective of these tests was to determine the effect of flow from the slots between fins in the upstream grain as the flow impacted the nonslotted downstream grain at the segment joint.

To conduct these tests, a special facility was constructed using a high-capacity industrial centrifugal blower. The blower was used to pull air through a ⅛-scale model (18-in.-diam) of the joint area.

Figure 2 shows the ignition-time model mounted to the blower via a diffuser. Flow entered the system through the bell-mouth sections shown, entering the core flow either directly via the center pipe or via the slots and holes in the finned-grain model. Figure 3 shows one of the fin or slot segments of the model, illustrating the exact placement of the ¼- and ⅛-in. holes used to simulate flow from the grain surface.

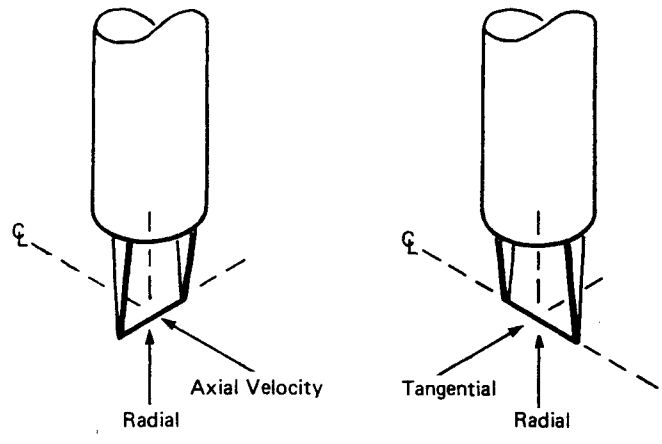

Fig. 6 Hot-wire alignments.

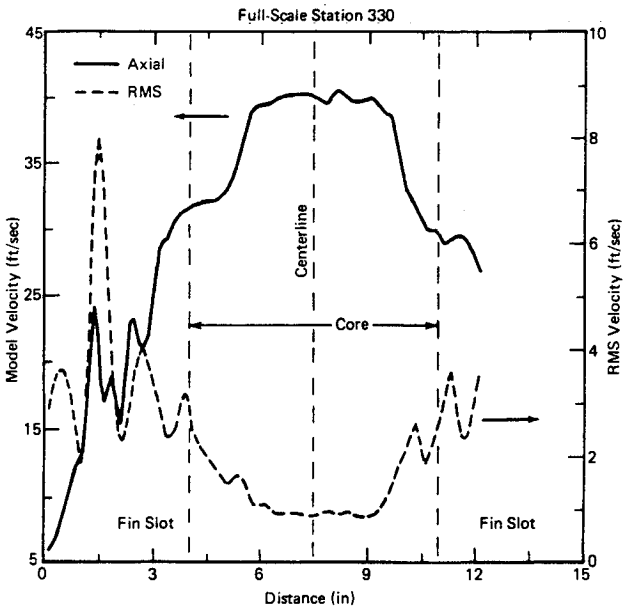

Fig. 7 Velocity profile upstream of joint.

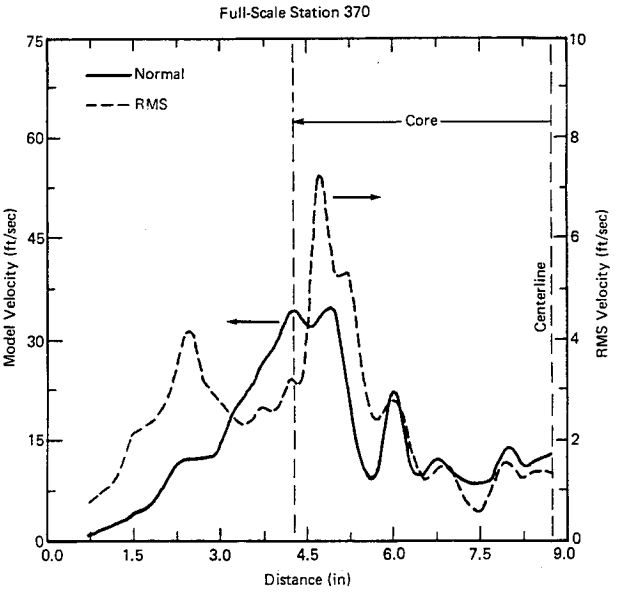

Fig. 10 Normal velocity profile in joint.

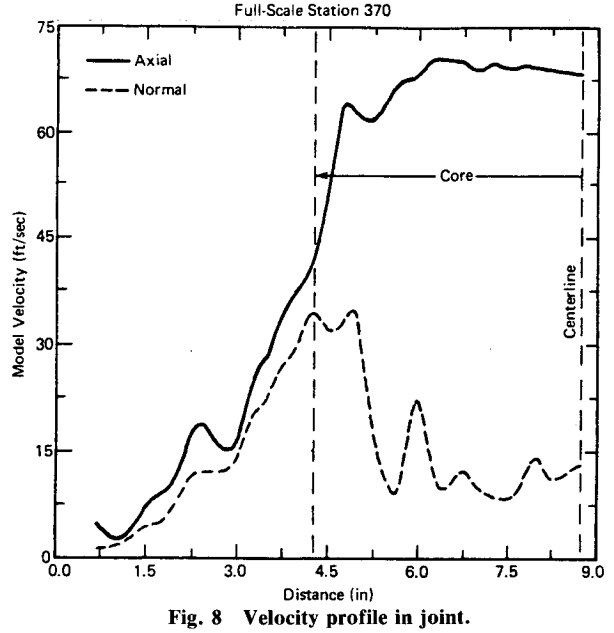

Fig. 8 Velocity profile in joint.

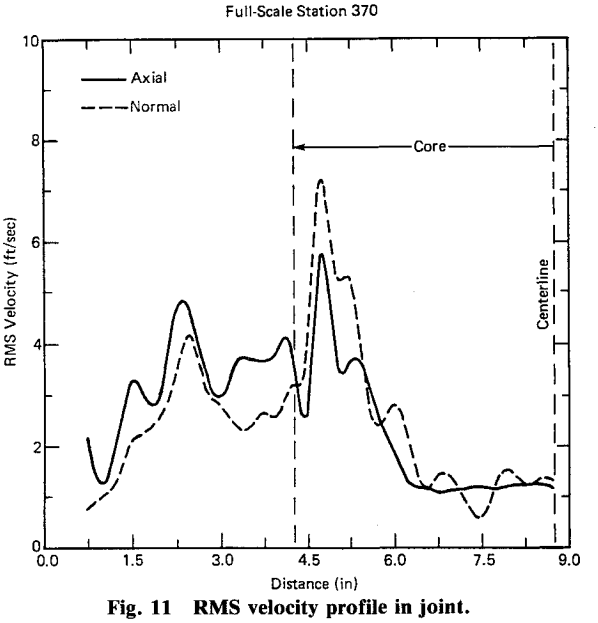

Fig. 11 RMS velocity profile in joint.

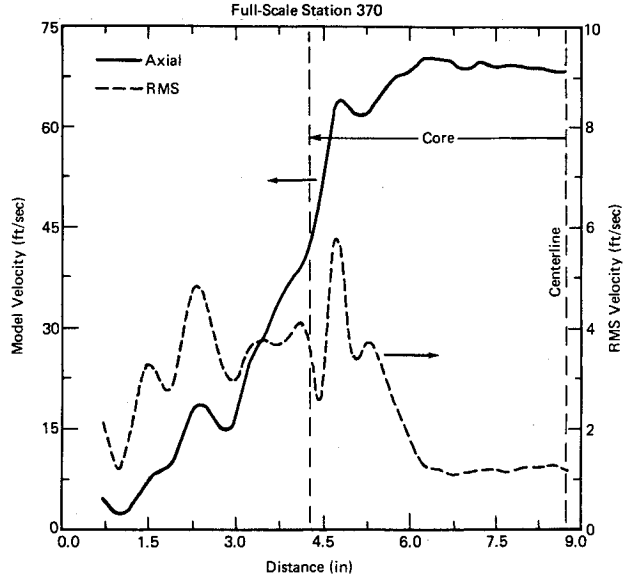

Fig. 9 Axial velocity profile in joint.

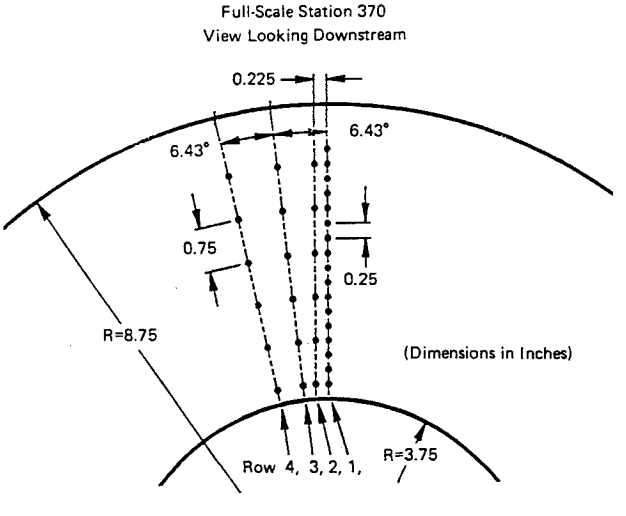

Fig. 12 Pressure tap distribution in joint.

Slightly over half of the fin length had holes to give a good representation of the flow introduced from stations 250–365; the latter is shown in Fig. 1 as the location of the forward joint in the full-scale SRM. The acrylic plate that modeled the base of the upstream segment grain at the joint is shown in Fig. 4. Hundreds of holes in this plate simulated the burning of the end of the upstream region grain at the joint itself. The need for the careful simulation of injected flow was demonstrated in Ref. 5 and applied in Refs. 6 and 7. Reynolds numbers, based on model parameters, are in the range of $3\text{–}4 \times 10^5$, within an order of magnitude of those in the full-scale design.

On the downstream side of the joint, the acrylic plate simulating the upstream face of the second segment grain was instrumented with pressure taps, as was the central core surface (Fig. 5). Pressure taps in these locations were connected to a scanning pressure-transducer system for mapping pressure distribution during tests. These pressure measurements, along with data from hot-wire anemometer scans in the SRM joint, comprised the test data. Note that the upstream and downstream grain faces at the joint could be rotated with respect to each other to allow a complete definition of pressures in the downstream grain surface at the joint as shown in Fig. 5.

Experimental Results

Before taking actual test data, measurements were made to ensure the correct modeling of the ratio of the mass flow through the core and through the fins. The mass-flow balance was performed by measuring velocity profiles upstream of the fins and downstream of the joint, calculating the mass-flow rates and the resulting ratios. These ratios were adjusted until they matched the ratios from the ballistic design code for the full-scale SRM. Pressure and velocity maps were made once the proper mass flow balance was achieved.

Ignition-Time Model

Velocity profiles were measured using a single hot-wire anemometer. There were two probe alignments during the radial traverses, as shown in Fig. 6. Radial and axial fluid motion contributed to the axial measurement when the probe was aligned perpendicular to the model's centerline axis, while tangential and radial components contributed to the transverse measured velocity. Figure 7 shows the hot-wire anemometer data taken upstream of the joint at a position approximately equivalent to station 330 on the full-scale SRM, i.e., 35 in. upstream of the joint. Shown in the figure is the axial velocity profile, both in the slot and in the core flow. As can be seen, there is a relatively flat velocity profile over about 5 in. of the core center; the velocity drops on either side of the

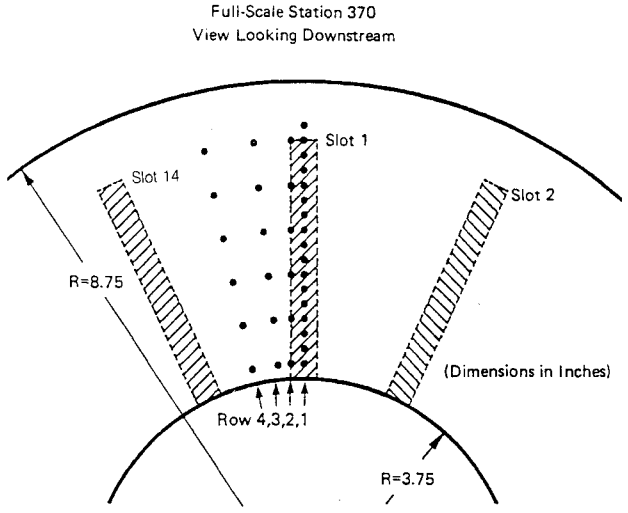

Fig. 13 Slot locations relative to pressure taps, case 1.

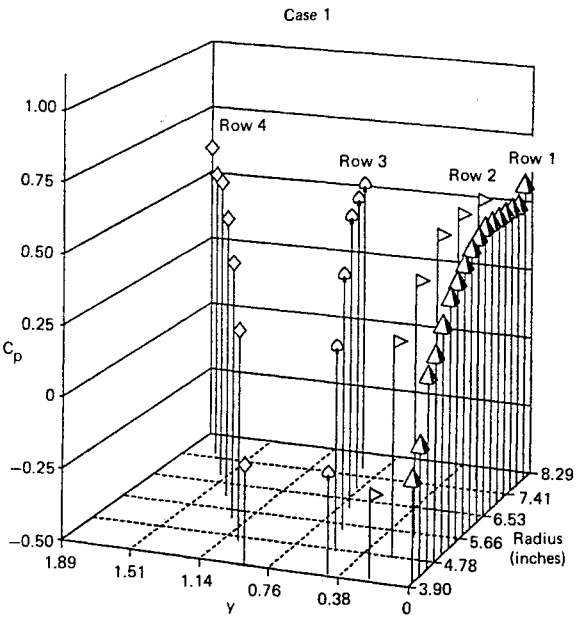

Fig. 14 C_p distribution in joint behind slot.

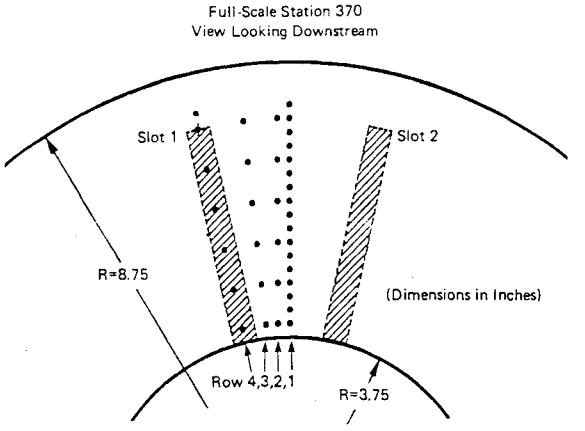

Fig. 15 Slot locations relative to pressure taps, case 2.

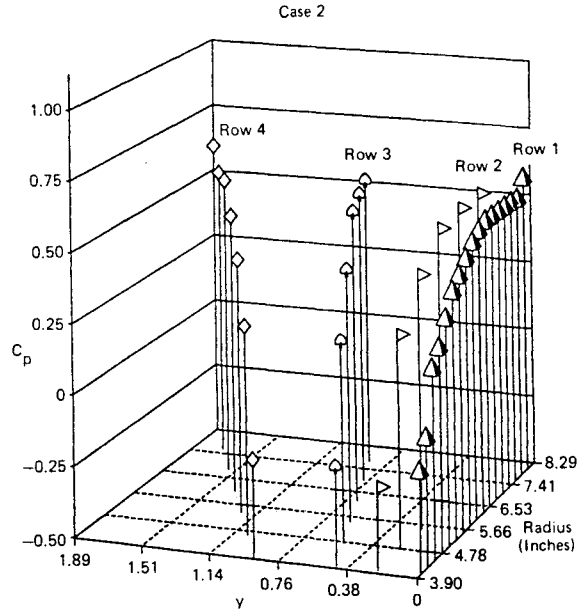

Fig. 16 C_p distribution in joint behind slot.

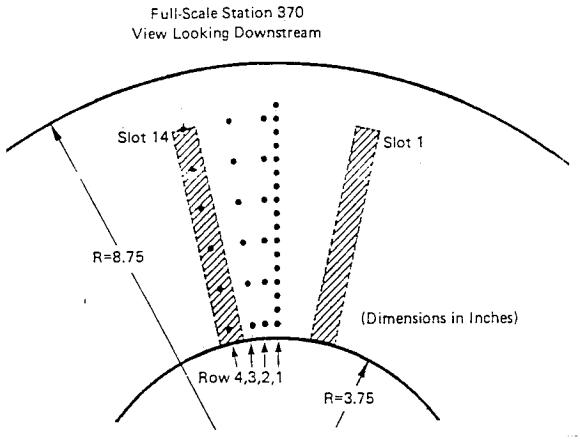

Fig. 17 Slot locations relative to pressure taps, case 3.

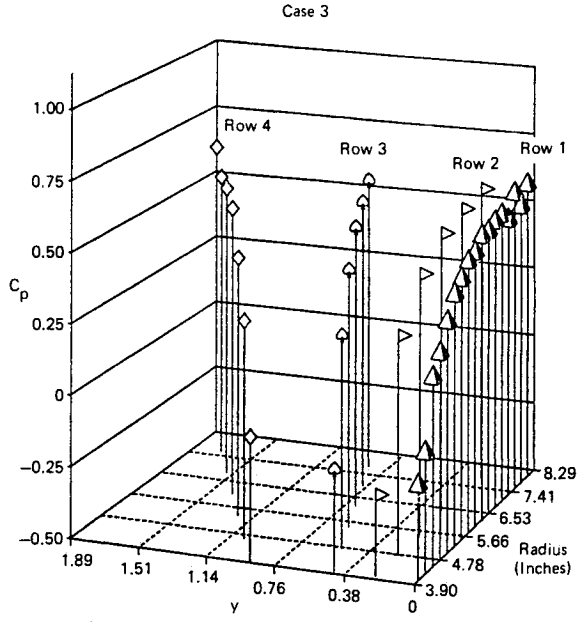

Fig. 18 C_p distribution in joint behind slot.

core as the slot area is approached. The thickness of the region where the velocity drops may indicate the extent to which the inertia of the injected gases disturbs the core flow. In the slot itself, the velocity drops steeply and then fluctuates rapidly about halfway into the slot before the velocity approaches zero at the base of the slot.

Figure 7 also shows the rms velocity data from the same traverses (note the different rms velocity scale on the right), indicating measured turbulence levels in the flow. This profile is almost a mirror image of the velocity plot with reduced turbulence in the core and increased turbulence in the slot. Note that at the position in the slot where there was considerable fluctuation in mean velocity, the turbulence level also takes a large jump. In this region, a substantial part of the so-called axial velocity is probably radial in direction; the rms velocity fluctuations may be as well.

Figures 8–11 show the velocity profiles in the joint. For these measurements, the hot-wire traverse was made with the wire in both the orientations shown in Fig. 6. One traverse was made with the wire itself perpendicular to the SRM axis. The resulting data are labeled as axial velocities in Figs. 8–11. The same comments regarding the flow components in Fig. 7 also apply to these figures.

Figure 8 shows that the core profile is similar to that seen upstream of the joint except that the velocity has increased due to the increase in mass flow in the core between the two measurement locations. The magnitude of the normal (radial) velocity component indicates the greatly increased level of nonaxial flow as the inner diameter of the fins is approached. The increase in nonaxial flow is indicative of the mixing process inherent in this region where the mass flow coming from the fin surface is mixing with the core flow. The similar profiles for the axial and normal flows in the region immediately downstream of the slot indicate that much of the flow in this region is probably radial, as the flow from the slot encounters the wall presented by the beginning of the second-segment grain and moves radially inward toward the core.

Figure 9 compares the previously shown axial flow data at the joint to their rms value or turbulence levels. Again, the rms velocity is plotted on a much exaggerated scale (right-hand side of figure). The increased turbulence near the edge of the fin again indicates the high level of mixing in this region.

The normal velocity and its associated level of turbulence are shown in Fig. 10. It is seen that in the core-flow area the rms velocity levels fluctuate in a manner similar to the mean velocities, whereas in the slot area the peak in rms velocity coincides with that seen for the rms results for the axial flow measurements. This indicates that the mixing in the area immediately downstream of the slot is random in direction.

The two rms velocity plots are compared in Fig. 11. While the plots show similar features, it is seen that the axial turbulence is somewhat dominant behind the slot while the normal turbulence activity is slightly dominant in the core. The fact that there are coincident peaks in the two curves at three locations indicates that the radial velocity component that they share dominates at those locations.

The pressure data for the tests were taken using the array of pressure taps in the face of the downstream grain segment shown in Fig. 12. In addition, a line of pressure taps was

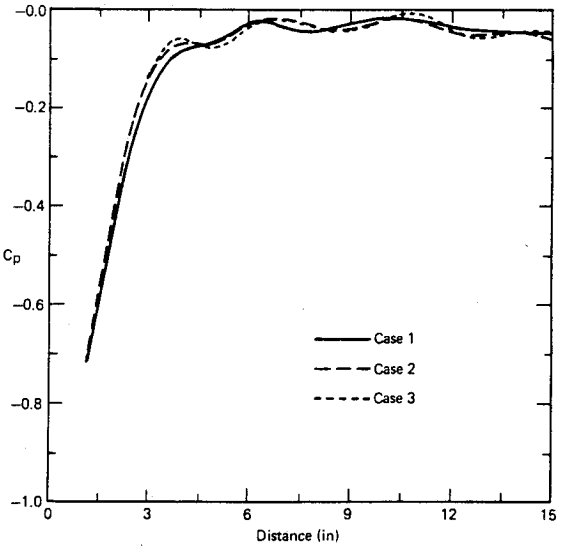

Fig. 19 C_p distribution downstream of joint.

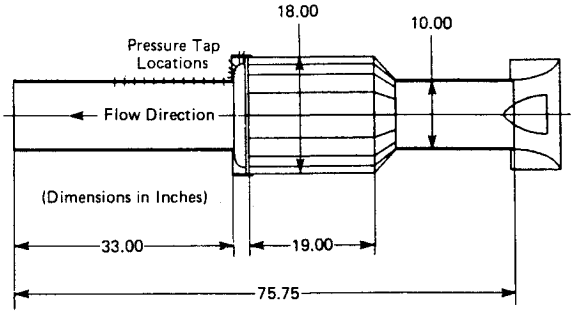

Fig. 20 Thirty-five-second model.

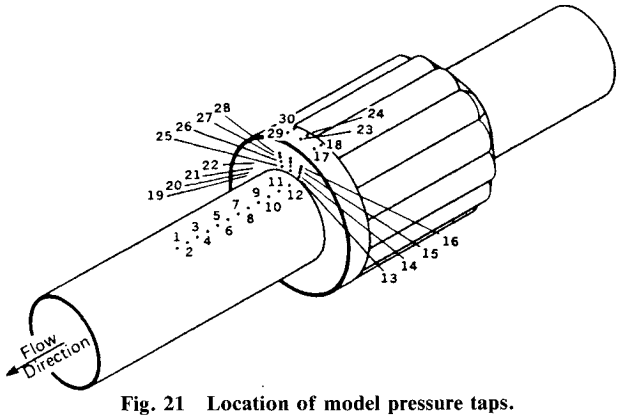

Fig. 21 Location of model pressure taps.

spaced over a 15-in. distance downstream of the slot, as indicated earlier in Fig. 5. The upstream grain model could be rotated to place the pressure taps shown in Fig. 12 in a variety of azimuthal positions downstream of a fin or slot.

The pressure data were recorded in terms of a pressure coefficient C_p where

$$C_p = \frac{p - p_\infty}{\frac{1}{2}\rho V_\infty 2}$$

Here the infinity (reference) position is at the centerline of the upstream core flow. Given this definition, absolute values of C_p have little meaning; relative values remain good indicators of the distribution of pressure and absolute velocity.

Figure 13 shows the tap orientation relative to a slot for one configuration (case 1), and Fig. 14 presents the corresponding pressure data (the rows are numbered as in Fig. 12). The ordinate labeled y gives the distance in inches of the tap from row 1. It is seen that the angular location of the pressure tap row relative to the upstream slot makes little difference in the shape of the pressure distribution. The plot shows that, as the outer wall is approached, the flow stagnates, and near the core, the flow is accelerating as it moves into the core. The absence of any real difference in C_p profiles among the rows of pressure taps indicates that the flow from the slots has spread rapidly into the joint area and that there is very little "slot" effect on the face of the downstream grain segment.

The results from the geometries labeled cases 2 and 3, where the main line of pressure taps is located between the slots, confirm the above results. The geometry for case 2 is shown in Fig. 15; the corresponding pressure distribution is shown in Fig. 16. The results are very close to those in Fig. 13. The pressure taps were placed behind two other slots in case 3, as seen in Fig. 17; once again, the pressure distributions (Fig. 18) are essentially identical to those shown in Fig. 13.

The pressures along the grain wall downstream of the joint are shown in Fig. 19. The results for all three cases are virtually identical and show that, within 6-8 in. downstream of the joint (in model scale), the flow has become axisymmetric.

These data indicate that any flow disturbances from the slots should have little effect on the flow over the grain in the second segment. Likewise, the data from the upstream face of the second segment indicate that the flow exiting from the slots will not have any untoward effect upon the design of the insulation/inhibitor on this face.

The tests reported in Refs. 1 and 2 represent the most complete data base of cold-flow testing to determine the effects of slots on core flow. Although no data directly comparable to those reported are given in those references, the effects of a comparable slot appeared to dissipate within a motor diameter.

Thirty-Five-Second Model

A depiction of the model representing the forward-segment grain at 35 s into the firing is given in Fig. 20. The pressure-tap locations are illustrated in Fig. 21.

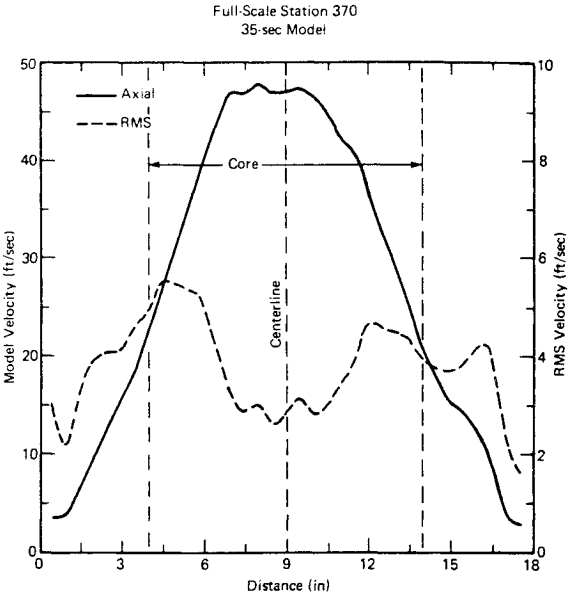

Fig. 22 Axial velocity profile in joint.

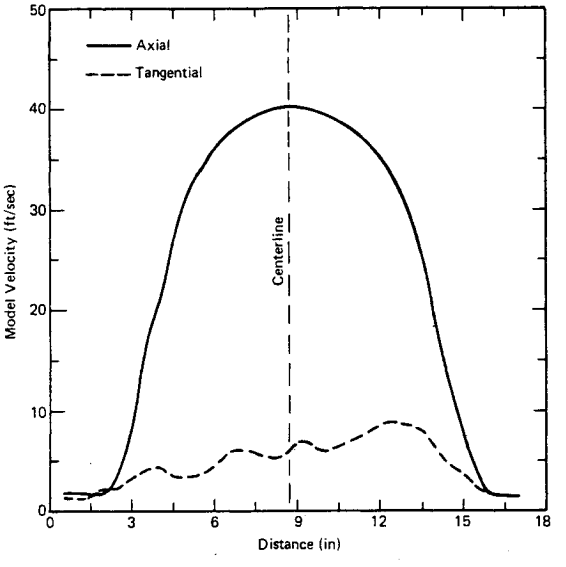

Fig. 23 Velocity distribution in joint.

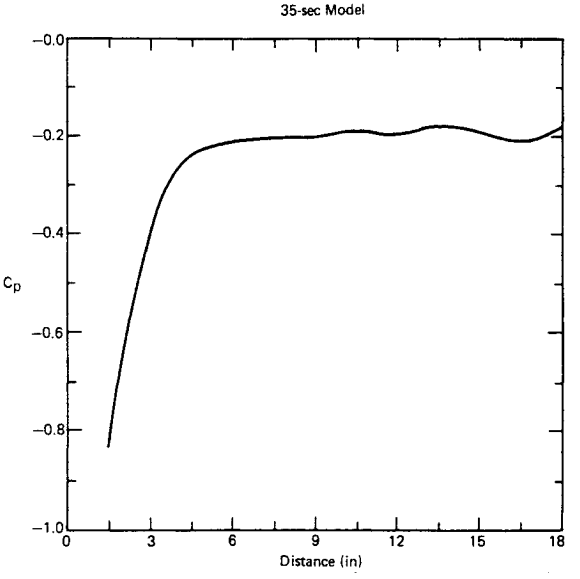

Fig. 24 C_p distribution downstream of joint.

Once again, the air-flow distribution was adjusted by means of a centerline cone in the upstream entrance to give the desired mass-flow balance between the upstream core flow and the finned-grain section. Pressures were measured on the upstream face of the second-segment grain and along the core surface of the second-segment grain to a distance 18 in. downstream of the joint. A hot-wire anemometer was again used to measure the velocity profile in the joint.

Figure 22 presents the velocity profile measured in the joint. Shown are profiles of the mean axial velocity (which also contains radial velocity components) and the rms profile. Note that the mean and rms profiles are plotted to different scales. As expected, the rms values are highest in the region where there is the greatest mixing of core flow with flow from the finned grain.

Figure 23 presents velocity results from the face of the second-segment grain. Comparable pressure coefficient data indicate that the flow essentially stagnates at the location of the third pressure tap in from the SRM wall along each row and then accelerates as it moves up the wall toward the second-segment core flow, reaching freestream velocity at the edge of the core. The pressures directly downstream of the fin stubs are slightly higher than those behind the slot, indicative of the lower velocities immediately behind the fins.

Figure 24 presents the pressure data along the surface of the grain model downstream of the joint in the second segment. The pressures indicate that the flow accelerates around the corner, separates, reattaches 3-4 in. (model scale) onto the second segment, and then becomes uniform further downstream. These results were confirmed by observing wool yarn tufts in that same area. As above, these data indicate that the effects of the slots on downstream flow dissipate rapidly.

Conclusions

The results of this series of cold-gas tests of a forward-slot grain have provided information for the ballistician and the insulation designer. In addition, they have reinforced the experience gained from several motors that have employed forward slots, viz., that the effects of such forward slots are minimal and can be quantified. The flow from the slots mixes rapidly (within less than a motor diameter) with the core flow so that the grain in the following segment is not subjected to an uneven flowfield. Equally important is the finding that there is no jetting from the slots impacting the forward face of the following segment, even at a small fraction of a motor diameter. In addition, there is no evidence of any tendency toward circumferential flow in the region between the two grain segments.

Acknowledgments

The assistance provided by W. Cowardin in fabricating the complex models required for these tests cannot be adequately recognized. In addition, C. Hetreed and P. Keitel assisted in recording data and in providing the CAD representations and data plots. They performed invaluable roles. This work was performed under Hercules-Atlantic funding.

References

[1]Dunlap, R., Blackner, A. M., Waugh, R. C., Brown, R. S., and Willoughby, P. G., "Internal Flow Field Studies in a Simulated Cylindrical Port Rocket Chamber," *Journal of Propulsion and Power*, Vol. 6, No. 6, pp. 690–704.

[2]Brown, R. S., Blackner, A. M., Willoughby, P. G., and Dunlap, R., "Coupling Between Velocity Oscillations and Solid Propellant Combustion," Chemical Systems Div., Sunnyvale, VA, Rept. F49620-84-C-0081, 1986.

[3]Waesche, W., Sargent, W. H., and Marchman, J. F., "Space Shuttle Solid Rocket Motor Aft-End Internal Flows," *Journal of Propulsion and Power*, Vol. 4, No. 6, 1989, pp. 650–657.

[4]Majumdor, A., and Whitesides, R. H., "Circumferential Flow Analysis in the Aft Field Joints of the Space Shuttle Solid Rocket Motor," *Journal of Propulsion and Power*, Vol. 5, No. 1, 1990, pp. 5–10.

[5]Taylor, G. I., "Fluid Flow in Regions Bounded by Porous Surfaces," *Proceedings of the Royal Society of London*, Vol. 234, 1956, pp. 456–475.

[6]Dunlap, R., Willoughby, P. G., and Hermsen, R. W., "Flowfield in the Combustion Chamber of a Solid Propellant Rocket Motor," *AIAA Journal*, Vol. 12, No. 10, 1974, pp. 1440–1442.

[7]Yamada, K., Goto, M., and Ishikawa, N., "Simulative Study of the Erosive Burning of Solid Rocket Propellants," *AIAA Journal*, Vol. 14, No. 9, 1976, pp. 1170–1176.